

Nuclear liquid-gas phase transition within a Brueckner-Hartree-Fock approach*

Jing Zhang(张晶)¹ Hong-Ming Liu(刘宏铭)¹ Zeng-Hua Li(李增花)^{1†} G. F. Burgio² H.-J. Schulze²

¹Institute of Modern Physics, Key Laboratory of Nuclear Physics and Ion-beam Application (MOE), Fudan University, Shanghai 200433, China

²INFN Sezione di Catania, Dipartimento di Fisica e Astronomia, Università di Catania, Via S. Sofia 64, I-95123 Catania, Italy

Abstract: The critical parameters of the liquid-gas phase transition of symmetric nuclear matter are computed using the Brueckner-Hartree-Fock method at finite temperature by employing different realistic nucleon-nucleon potentials. Temperature effects on single-particle potentials, defect functions, and three-body forces are discussed in detail. Results obtained from the full procedure and frozen-correlations approximation are compared. We find critical temperatures of approximately 14 to 19 MeV and critical densities in the range of 0.05 to 0.08 fm⁻³, depending on the interactions employed.

Keywords: nuclear liquid-gas phase transition, Brueckner-Hartree-Fock approach, symmetric nuclear matter

DOI: 10.1088/1674-1137/ac82e2

I. INTRODUCTION

The nucleonic equation of state (EOS) at finite temperature provides basic knowledge on the study of nuclear structure [1], compact stars [2, 3], and heavy-ion collisions [4–6]. In particular, the liquid-gas phase transition [7–11] calculated using the EOS of symmetric nuclear matter at finite temperature is required to analyze the properties of nuclear matter in different phases [12–14], such as phenomena related to the evolution of neutron stars and heavy ion collisions [15].

At comparatively low temperatures $T \lesssim 10$ MeV and densities $\rho \lesssim 0.1$ fm⁻³, the coexistence of liquid and vapor phases occurs in nuclear matter, resulting from the properties of the nucleon-nucleon interaction [16], which is similar to the van-der-Waals behavior in condensed matter physics. The thermodynamic quantities of liquid-gas coexistence, such as critical temperature T_c , critical pressure p_c , and critical density ρ_c , are generally referred to as critical parameters. In the past, they have been investigated both in heavy-ion-collision experiments [17–19] and different theoretical models [20–43], and the results have been extrapolated to finite nuclei. Critical temperatures in the range $T_c \approx 13–22$ MeV were deduced.

In different experiments, critical parameters have been studied by measuring caloric curves and analyzing the multi-fragment distribution of heavy-ion collisions.

The limiting temperature T_{\lim} is the maximum temperature that can be observed in experiments. It is not equal to T_c owing to the existence of the Coulomb repulsion and surface tension of finite nuclei. However, there is still a relatively stable ratio between T_c and T_{\lim} [28]. In a combined analysis of several experiments [35], under different excitation energies and extrapolation using the droplet model, the critical parameters were estimated as $T_c = 17.9 \pm 0.4$ MeV, $\rho_c = 0.06 \pm 0.02$ fm⁻³, and $p_c = 0.31 \pm 0.07$ MeV fm⁻³ for infinite symmetric nuclear matter, in agreement with an earlier analysis giving $T_c = 16.6 \pm 0.9$ MeV [27].

In this theoretical study of the liquid-gas phase, we employ the Brueckner-Hartree-Fock (BHF) model [1, 44–46] extended to finite temperature [47, 48]. Previously [24, 26], a critical temperature of $T_c \approx 20$ MeV was obtained using this method with the bare Paris potential [49] or the Argonne V₁₄ potential [50] supplemented with phenomenological three-body forces (TBF) [51]. The liquid-gas transition disappeared at isospin asymmetry of approximately 0.9. A slightly lower value $T_c \approx 18$ MeV was found in [28] with the Bonn B potential [52], and $T_c \approx 13$ MeV was obtained with the V₁₈ potential and updated TBF in [29, 53]. All these BHF values are significantly higher than $T_c \approx 10$ MeV deduced with the Dirac-Brueckner-Hartree-Fock (DBHF) approach in Refs. [22, 25]. In the BHF approach, the inclusion of suitable TBF

Received 16 June 2022; Accepted 21 July 2022; Published online 25 August 2022

* Sponsored by the National Natural Science Foundation of China (11975077, 11475045), "PHAROS", COST Action CA16214 and the agreement ASI-INAF n.2017-14-H.O

† E-mail: zhli09@fudan.edu.cn

©2022 Chinese Physical Society and the Institute of High Energy Physics of the Chinese Academy of Sciences and the Institute of Modern Physics of the Chinese Academy of Sciences and IOP Publishing Ltd

is essential to obtain a realistic saturation point for nuclear matter and thus produce well-founded predictions for T_c .

The liquid-gas phase transition has also been investigated using other theoretical methods. The first Skyrme [20] and variational [21, 26] calculations reported values in the range $T_c \approx 16 - 19$ MeV. In the framework of covariant-density-functional theory, values of 20 different models were recently compared and predicted as $T_c \approx 13 - 16$ MeV [38], in agreement with those of several relativistic-mean-field models [30, 32–34, 41–43]. Self-consistent Green function (SCGF) calculations with the V₁₈ potential predicted $T_c = 11.6$ MeV [54], and a recent comparison of SCGF [39] and BHF results using different chiral interactions yielded $T_c = 16 \pm 2$ MeV [37], with the difference between the two methods using the same chiral interaction being less than 2 MeV. In the framework of in-medium chiral perturbation theory [55], $T_c \approx 15$ MeV was obtained for isospin-symmetric nuclear matter. Finite nuclei with isospin asymmetry of approximately 0.13 were analyzed within an isospin-dependent quantum molecular dynamics model [40]. Extrapolating the critical temperature to infinite nuclear matter yielded a value of $T_c \approx 13.3 \pm 1.2$ MeV.

In this paper, we employ the BHF method based on several realistic nucleon-nucleon (NN) interactions, namely Argonne V₁₈ (V18) [56], Bonn B (BOB) [52], and Nijmegen 93 (N93) [57] potentials, supplemented by compatible microscopically-derived TBF [58–61] and a combination of the V₁₈ potential and the phenomenological Urbana-type TBF [51, 62], which is labeled as UIX. The compatibility of the resulting zero-temperature EOSs with nuclear-structure phenomenology [63–65] and recent astronomical observation constraints [66–68] has been studied in several publications.

The paper is organized as follows. In Sec. II, we briefly review the BHF method at finite temperature and the computation of thermodynamic quantities. In Sec. III, we present the results of the procedure used in this study and compare them with previous results in detail, regarding, in particular, the critical parameters. Finally, conclusions are drawn in Sec. IV.

II. FORMALISM

Calculations for infinite symmetric nuclear matter are based on Brueckner-Bethe-Goldstone (BBG) theory [44, 45, 69–71] and its extension to finite temperature [26, 29, 47, 48, 72, 73]. In this study, we adopt the four types of interaction V mentioned above to obtain the free energy per particle to analyze the liquid-gas phase transition of hot nuclear matter. The fundamental ingredient of BBG theory is the K matrix, which represents the effective interaction between nucleons in nuclear matter and obeys the integral equation

$$K(\rho, x_p; E) = V + V \operatorname{Re} \sum_{1,2} \frac{|12\rangle(1-n_1)(1-n_2)\langle 12|}{E - e_1 - e_2 + i0} \times K(\rho, x_p; E), \quad (1)$$

where E is the starting energy, and the multiple indices 1, 2 represent momentum, isospin, and spin. Along with the equations for single-particle (s.p.) energy and potential,

$$e_1 = \frac{k_1^2}{2m_1} + U_1, \quad (2)$$

$$U_1(\rho, x_p) = \sum_a n_2 \langle 12 | K(\rho, x_p; e_1 + e_2) | 12 \rangle_a, \quad (3)$$

the K matrix can be obtained self-consistently for a given baryon density ρ and proton fraction x_p . The numerical diagonalization of the BBG equation (1) keeps track of the total and relative momenta and starting energy E while retaining the excellent angle-average approximation [74–76].

The TBF are reduced to an effective, density-dependent, two-body force by averaging over the third nucleon in the medium [61],

$$\bar{V}_{12}(\mathbf{r}_{12}) = \rho \int d^3\mathbf{r}_3 \sum_{\sigma_3, \tau_3} g_{13}(r_{13})^2 g_{23}(r_{23})^2 V_{132}, \quad (4)$$

the average being weighted by the BHF correlation function $g_\alpha(r) = 1 - \eta_\alpha(r)$, related to the r -space defect functions in the partial waves α ,

$$\eta_\alpha(r) = j_\alpha(r) - u_\alpha(r), \quad (5)$$

with the free wave function (Bessel function) j_α , and the correlated wave function u_α , which consider nucleon-nucleon in-medium correlations [26, 58–60, 77–81]. The result is an effective two-nucleon potential with the operator structure

$$\begin{aligned} \bar{V}_{12}(\mathbf{r}) = & (\boldsymbol{\tau}_1 \cdot \boldsymbol{\tau}_2)(\boldsymbol{\sigma}_1 \cdot \boldsymbol{\sigma}_2)V_C(r) + (\boldsymbol{\sigma}_1 \cdot \boldsymbol{\sigma}_2)V_S(r) + V_I(r) \\ & + S_{12}(\hat{\mathbf{r}})[(\boldsymbol{\tau}_1 \cdot \boldsymbol{\tau}_2)V_T(r) + V_Q(r)], \end{aligned} \quad (6)$$

where $S_{12}(\hat{\mathbf{r}}) = 3(\boldsymbol{\sigma}_1 \cdot \hat{\mathbf{r}})(\boldsymbol{\sigma}_2 \cdot \hat{\mathbf{r}}) - \boldsymbol{\sigma}_1 \cdot \boldsymbol{\sigma}_2$ is the tensor operator, and the five components V_O , $O = C, S, I, T, Q$ depend on the nucleon densities ρ_n, ρ_p . These are all added to the bare two-nucleon potential in the Bethe-Goldstone equation.

Eqs. (1)–(3) involve the Fermi distribution $n(k)$ and must be solved self-consistently along with the equation for the auxiliary chemical potentials $\tilde{\mu}_i$ ($i = n, p$) fixing the density,

$$\rho_i = 2 \sum_k n_i(k) = 2 \sum_k \left[\exp\left(\frac{e_i(k) - \tilde{\mu}_i}{T}\right) + 1 \right]^{-1}. \quad (7)$$

The results of this iterative procedure are temperature-dependent s.p. potentials $U_i(k)$, which are then used to compute the free energy density for a given temperature and density.

$$f = \rho \frac{F}{A} = \sum_{i=n,p} \left[2 \sum_k n_i(k) \left(\frac{k^2}{2m_i} + \frac{1}{2} U_i(k) \right) - T s_i \right], \quad (8)$$

where

$$s_i = -2 \sum_k \left(n_i(k) \ln n_i(k) + [1 - n_i(k)] \ln [1 - n_i(k)] \right) \quad (9)$$

is the entropy density of a free Fermi gas with the s.p. spectrum $e_i(k)$.

In previous studies, a further "frozen-correlations" approximation (FCA) was sometimes employed [26, 82–84], in which the temperature dependence of the s.p. potential $U_i(k)$ is neglected and the free energy in Eq. (8) is computed using the zero-temperature s.p. potential. In the following, we compare the results of the full procedure (termed BHF) and the FCA.

The free energy density allows us to compute, in a thermodynamically consistent manner, other thermodynamic quantities of interest, namely chemical potentials μ_i , pressure p , and internal energy density ε ,

$$\mu_i = \frac{\partial f}{\partial \rho_i}, \quad (10)$$

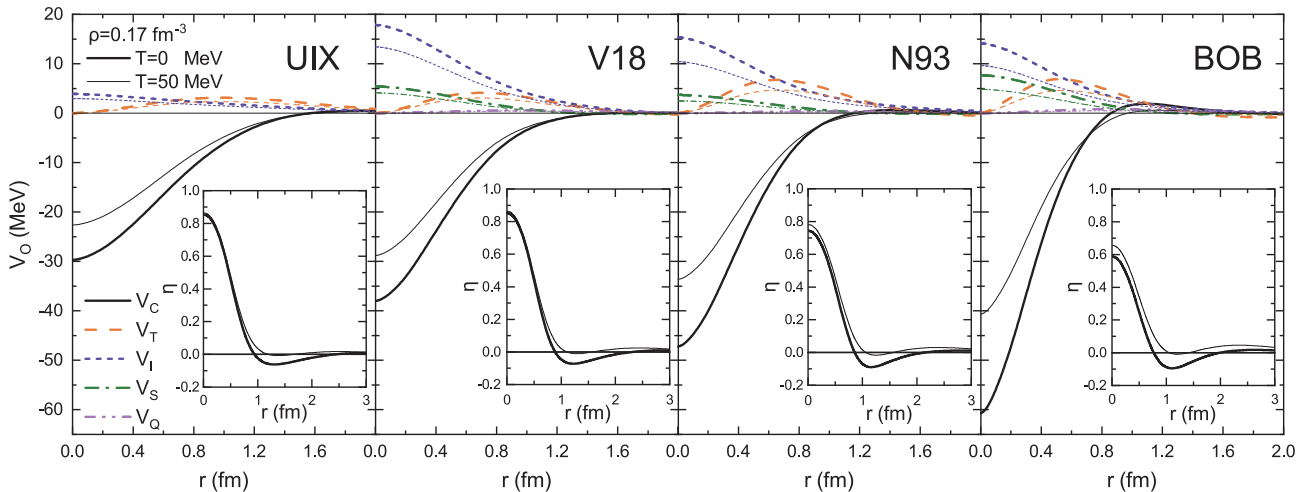


Fig. 1. (color online) TBF components (Eq. (6)) for $\rho = 0.17 \text{ fm}^{-3}$, $T = 0$ and 50 MeV with different EOSs. The insets show the defect functions in the 1S_0 channel.

$$p = \rho^2 \frac{\partial(f/\rho)}{\partial \rho} = \sum_i \mu_i \rho_i - f, \quad (11)$$

$$\varepsilon = f + T s, \quad s = -\frac{\partial f}{\partial T}. \quad (12)$$

In particular, the pressure is analyzed in the following discussion of the critical point.

III. RESULTS

We now discuss the results of our numerical calculations following the BHF and FCA procedures. The latter entirely disregards the T dependence of the s.p. properties and is thus a good reference for the quantitative importance of these effects.

A. Temperature effects on single-particle properties

To illustrate the iterative BHF procedure that fully includes Fermi distributions at finite temperature in the computation of the K matrix, Eq. (1), and the s.p. potential U (Eqs. (2) and (3)), we now discuss the temperature dependence of several physical quantities of interest.

In Fig. 1, we display the five TBF components in Eq. (6) obtained at normal density $\rho = 0.17 \text{ fm}^{-3}$, $T = 0$, and 50 MeV with different interactions. The (π, ρ) -exchange TBF contribute to the attractive central (V_C) and tensor (V_T) components, whereas the (σ, ω) TBF are mainly represented by the repulsive scalar (V_I) component [60]. The other two parts, V_S and V_Q , are less important. For the phenomenological UIX that only involve 2π exchange, the contributions from these two parts are zero. One can clearly see that the five components depend quantitatively on the EOS and are all weakened at finite temperature.

The only way finite temperature affects the effective

TBF in our formalism is via the correlation functions $g_\alpha = 1 - \eta_\alpha$ in Eq. (4) that are obtained consistently from the K matrix [80, 81]. For illustration, the insets of Fig. 1 show the defect functions η_{S_0} for the same conditions as the TBF in the figure. We can see that (for the 'soft-core' EOSs N93 and BOB in particular [80]) finite temperature increases the defect function and thus decreases the correlation functions g in Eq. (4), which explains the decrease in the average TBF. In other words, at finite T , interacting nucleons are maintained at larger distances, and the effective 'core' of the NN interaction increases.

This repulsive effect is also observed in the s.p. potentials, which are shown in Fig. 2(a) at $T = 0$ and 20 MeV for $\rho = 0.06$ (left panels) and $\rho = 0.17$ fm $^{-3}$ (right panels), with the four EOSs. The change due to finite temperature ($\Delta U \equiv U_T - U_0$) is shown in the central panels (b), and the Fermi distributions for the BHF and FCA procedures are shown in the lower panels (c) only for V18. It is evident that finite temperature generally increases U and ΔU (the FCA corresponds to $\Delta U = 0$), thus providing effective repulsion and increasing the free en-

ergy (Eq. (8)). However, there are exceptions, such as N93 at $\rho = 0.17$ fm $^{-3}$, which becomes more attractive at $T = 20$ MeV. This temperature effect is due to the use of Fermi functions in Eqs. (1), (2), and (3), as well as the T dependence of the TBF (see Fig. 1), which weakens the individual components. We verify that the particular behavior of N93 is due to the finite- T modification of the TBF, which provides more attraction in this case, in contrast to the other EOSs.

However, there are several delicate effects from the different momentum distributions involved in the BHF and FCA procedures, which are caused by the use of s.p. spectra at (non)zero temperature, respectively. Note that in Fig. 2(c), the momentum distribution in the BHF procedure is slightly less extended; therefore, the kinetic-energy contribution E_c/A to F/A (first term in Eq. (8)) is smaller than that in the FCA. This counteracts the general increase in the potential contribution E_U/A (second term in Eq. (8)) in the BHF discussed above. Furthermore, the entropy contributions TS/A (third term in Eq. (8)) are slightly different in the BHF and FCA proced-

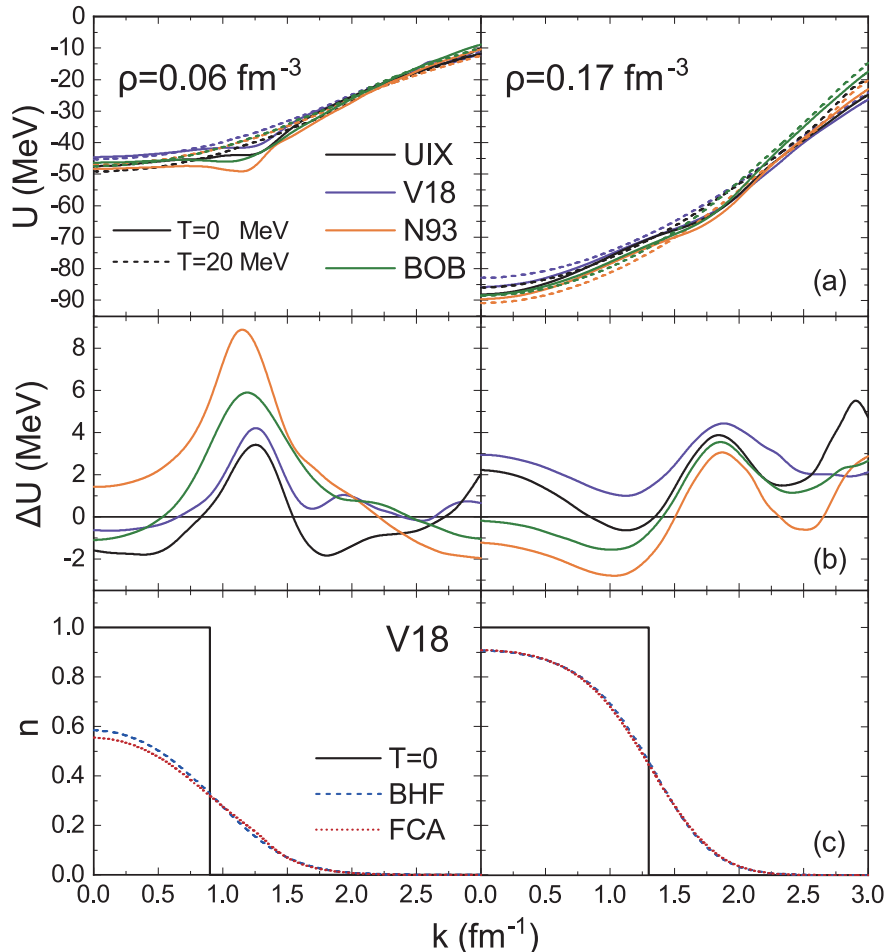


Fig. 2. (color online) (a) Self-consistent s.p. potential at $T = 0$ and 20 MeV for $\rho = 0.06$ and $\rho = 0.17$ fm $^{-3}$ with different EOSs. (b) Differences in U between $T = 20$ MeV and $T = 0$ MeV. (c) Momentum distributions from the BHF and FCA procedures for the V18 EOS.

Table 1. Contributions to F/A (in MeV) at $\rho = 0.17 \text{ fm}^{-3}$ and $T = 20 \text{ MeV}$ in the BHF and FCA procedures.

		F/A	E_c/A	E_U/A	TS/A
UIX	BHF	-34.0	33.6	-35.9	31.7
	FCA	-34.5	34.3	-36.2	32.6
V18	BHF	-33.1	33.9	-34.9	32.1
	FCA	-34.2	34.4	-35.8	32.8
N93	BHF	-35.9	33.1	-38.0	31.0
	FCA	-35.4	34.0	-37.2	32.2
BOB	BHF	-34.9	32.9	-37.1	30.7
	FCA	-34.9	33.7	-36.8	31.8

ures, which is summarized in Table 1 at $\rho = 0.17 \text{ fm}^{-3}$ and $T = 20 \text{ MeV}$. Under these conditions, the decrease in the kinetic-energy contribution in the BHF procedure is less than 1 MeV for all EOSs, which is compensated in all cases by a comparable opposite change in the entropy contribution. In contrast, the potential contribution is EOS dependent, varying from repulsive (V18) to attractive (N93), as shown in Fig. 2(b). In the end, the overall change in F/A under the BHF procedure ranges from slightly repulsive (UIX,V18) to attractive (N93), which is the result of a delicate compensation between different contributions and changes with density and temperature.

The final results of the free energy per particle for a given temperature and density with different EOSs are shown in Fig. 3, comparing the BHF and FCA procedures. We may conclude that the difference between both procedures is rather small over the full range of parameters and may have either sign owing to the various compensation mechanisms stated above. These results allow the computation of the pressure (Eq. (11)) and thus the following analysis of the critical point.

B. Critical point of symmetric nuclear matter

In the study of the liquid-gas phase transition, the critical parameters T_c , ρ_c , and p_c determine the properties in the vicinity of the phase transition. The pressure $p(\rho)$ determined by the BHF procedure is depicted in Fig. 4 for different values of temperature (dashed green curves), comprising the proper value T_c for each EOS (solid black curves). The results range from $T_c = 14.4 \text{ MeV}$ for V18 to $T_c = 19.2 \text{ MeV}$ for the N93 EOS and are also listed in Table 2 along with the corresponding values of ρ_c and p_c . The results of the BHF and FCA procedures are similar, as also evidenced in Fig. 3, but reflect qualitatively the different behaviors for ΔU shown in Fig. 2(b), that is, T_c in the BHF is higher (lower) than in the FCA for the N93 (UIX, V18, and BOB) EOS. In any case, these values compare well with the recent experimental and theoretical results discussed in the Introduction. However, the results for p_c are not well constrained, ranging from 0.25 to 0.63 MeV fm^{-3} .

Table 2. Parameters of the critical point for symmetric nuclear matter with different EOSs from the BHF and FCA procedures.

		T_c/MeV	ρ_c/fm^{-3}	$p_c/(\text{MeV fm}^{-3})$
UIX	BHF	15.1	0.053	0.29
	FCA	15.2	0.067	0.39
V18	BHF	14.4	0.062	0.29
	FCA	15.6	0.065	0.41
N93	BHF	19.2	0.051	0.31
	FCA	17.2	0.076	0.63
BOB	BHF	15.3	0.050	0.25
	FCA	15.9	0.070	0.52

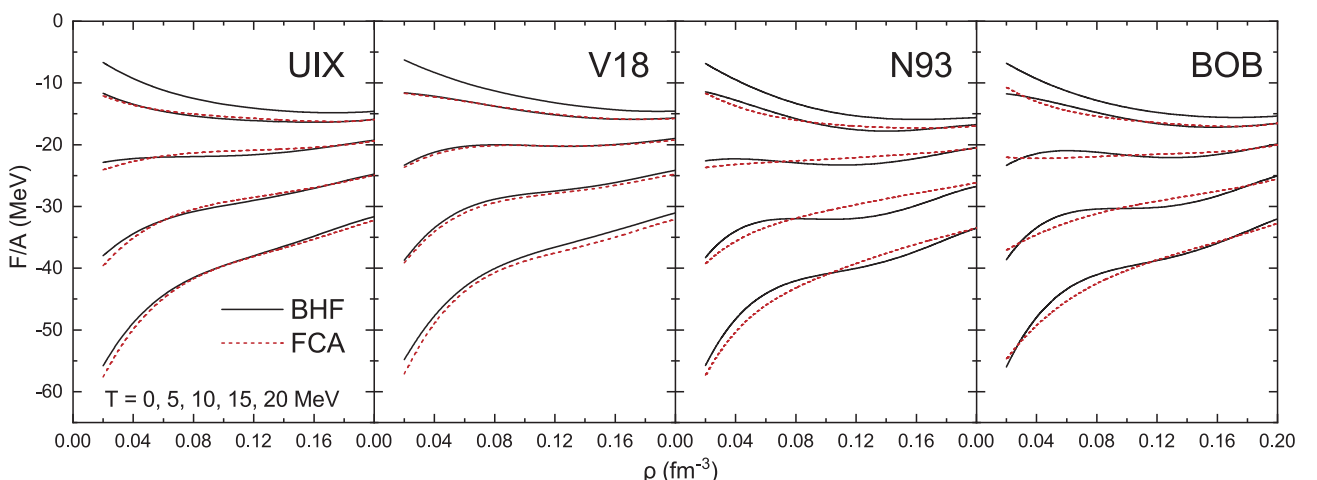


Fig. 3. (color online) Free energy per nucleon as a function of density for various temperatures with different EOSs obtained with the BHF or FCA procedures.

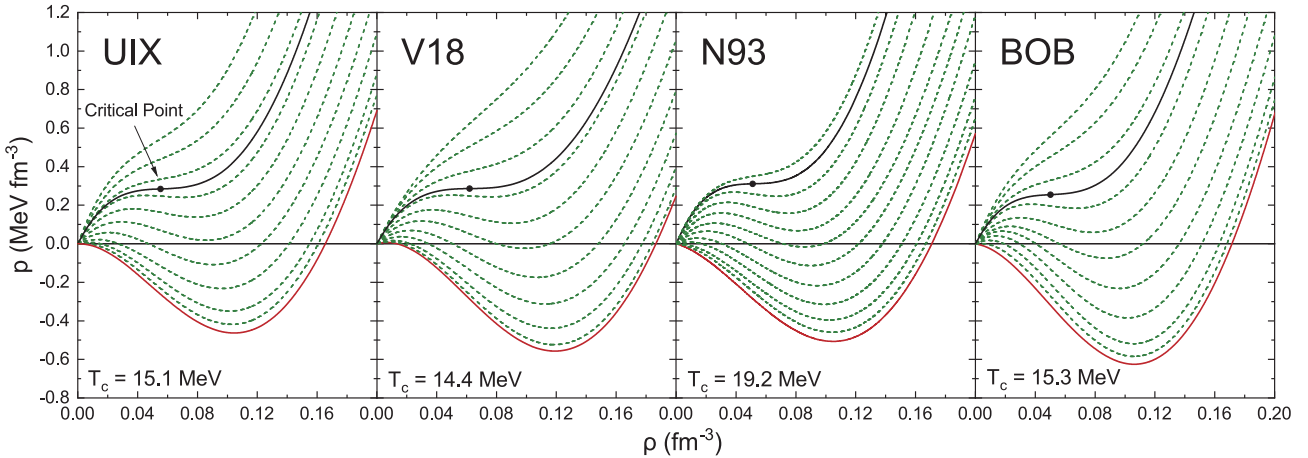


Fig. 4. (color online) Pressure of symmetric nuclear matter as a function of density for various temperatures $T = 0, 2, 4, \dots, 20$ MeV (rising curves) with different EOSs and the BHF procedure. The solid black curves correspond to the critical temperatures T_c , and the critical points are denoted by markers.

IV. SUMMARY

We compute the critical parameters of symmetric nuclear matter in the BHF formalism with several realistic EOSs, comparing in detail two procedures with and without consideration of the temperature dependence of s.p. energies.

Considering all cases, the critical temperatures are found in the range $T_c \approx 14 - 19$ MeV, and critical densities are found in the range $\rho_c \approx 0.05 - 0.08$ fm $^{-3}$, which are in good agreement with the available experimental results and the results of other theoretical approaches, apart from the DBHF model, which has predicted significantly smaller values. In our case, the variation in results is due to different two- and three-body forces used as the input to the BHF scheme. Although all of them provide similar

realistic saturation properties for nuclear matter, the wide range of results for the critical properties may be considered as a current theoretical uncertainty regarding the construction of many-body input forces for the BHF scheme.

The finite- T extension of the BHF formalism used here comprises temperature effects arising from the Fermi distribution functions in the Pauli operator and momentum integrals, whereas the input two- and three-body forces are assumed temperature independent. A consistent inclusion of temperature effects in these quantities has not yet been attempted and is a serious theoretical challenge for the future, because we show that the predicted critical point depends on the two- and three-body forces employed.

References

- [1] M. Baldo and G. F. Burgio, *Rep. Prog. Phys.* **75**, 026301 (2012)
- [2] J. M. Lattimer and M. Prakash, *Phys. Rep.* **621**, 127 (2016)
- [3] G.-F. Burgio, H.-J. Schulze, I. Vidaña *et al.*, *Prog. Part. Nucl. Phys.* **120**, 103879 (2021)
- [4] P. Danielewicz, R. Lacey, and W. G. Lynch, *Science* **298**, 1592 (2002)
- [5] B.-A. Li, L.-W. Chen, and C. M. Ko, *Phys. Rep.* **464**, 113 (2008)
- [6] M. B. Tsang *et al.*, *Phys. Rev. C* **86**, 015803 (2012)
- [7] D. Q. Lamb, J. M. Lattimer, C. J. Pethick *et al.*, *Phys. Rev. Lett.* **41**, 1623 (1978)
- [8] G. Bertsch and P. J. Siemens, *Phys. Lett. B* **126**, 9 (1983)
- [9] J. Kapusta, *Phys. Rev. C* **29**, 1735 (1984)
- [10] H. R. Jaqaman, A. Z. Mekjian, and L. Zamick, *Phys. Rev. C* **29**, 2067 (1984)
- [11] S. J. Lee and A. Z. Mekjian, *Phys. Rev. C* **63**, 044605 (2001)
- [12] K. A. Brueckner, S. A. Coon, and J. Dabrowski, *Phys. Rev.* **168**, 1184 (1968)
- [13] P. J. Siemens, *Nucl. Phys. A* **141**, 225 (1970)
- [14] J. Blaizot, *Phys. Rep.* **64**, 171 (1980)
- [15] P. J. Siemens, *Nature* **305**, 410 (1983)
- [16] M. E. Fisher, *Physics Physique Fizika* **3**, 255 (1967)
- [17] J. E. Finn *et al.*, *Phys. Rev. Lett.* **49**, 1321 (1982)
- [18] J. Pochodzalla *et al.*, *Phys. Rev. Lett.* **75**, 1040 (1995)
- [19] V. A. Karnaukhov *et al.*, *Phys. of Atomic Nucl.* **71**, 2067 (2008)
- [20] J. M. Lattimer and D. G. Ravenhall, *Astrophys. J.* **223**, 314 (1978)
- [21] B. Friedman and V. R. Pandharipande, *Nucl. Phys. A* **361**, 502 (1981)
- [22] B. ter Haar and R. Malfliet, *Phys. Rev. Lett.* **56**, 1237 (1986)
- [23] R. K. Su, S. D. Yang, and T. T. S. Kuo, *Phys. Rev. C* **35**, 1539 (1987)
- [24] M. Baldo, I. Bombaci, L. S. Ferreira *et al.*, *Phys. Lett. B* **215**, 19 (1988)

- [25] H. Huber, F. Weber, and M. K. Weigel, *Phys. Rev. C* **57**, 3484 (1998)
- [26] M. Baldo and L. S. Ferreira, *Phys. Rev. C* **59**, 682 (1999)
- [27] J. B. Natowitz, K. Hagel, Y. Ma *et al.*, *Phys. Rev. Lett.* **89**, 212701 (2002)
- [28] M. Baldo, L. S. Ferreira, and O. E. Nicotra, *Phys. Rev. C* **69**, 034321 (2004)
- [29] W. Zuo, Z. H. Li, A. Li *et al.*, *Phys. Rev. C* **69**, 064001 (2004)
- [30] P. K. Sahu, T. K. Jha, K. C. Panda *et al.*, *Nucl. Phys. A* **733**, 169 (2004)
- [31] V. Somà and P. Božek, *Phys. Rev. C* **80**, 025803 (2009)
- [32] S. Typel, G. Röpke, T. Klähn *et al.*, *Phys. Rev. C* **81**, 015803 (2010)
- [33] C. Wu and Z. Ren, *Phys. Rev. C* **83**, 044605 (2011)
- [34] G.-H. Zhang and W. Jiang, *Phys. Lett. B* **720**, 148 (2013)
- [35] J. B. Elliott, P. T. Lake, L. G. Moretto *et al.*, *Phys. Rev. C* **87**, 054622 (2013)
- [36] S. Zaryouni, M. Hassani, and H. R. Moshfegh, *Phys. Rev. C* **89**, 014332 (2014)
- [37] A. Carbone, A. Polls, and A. Rios, *Phys. Rev. C* **98**, 025804 (2018)
- [38] S. Yang, B. N. Zhang, and B. Y. Sun, *Phys. Rev. C* **100**, 054314 (2019)
- [39] A. Carbone and A. Schwenk, *Phys. Rev. C* **100**, 025805 (2019)
- [40] H. L. Liu, Y. G. Ma, and D. Q. Fang, *Phys. Rev. C* **99**, 054614 (2019)
- [41] V. Parmar, M. K. Sharma, and S. K. Patra, *J. Phys. G* **48**, 025108 (2021)
- [42] A. Kumar, H. C. Das, S. K. Biswal *et al.*, *EPJC* **80**, 775 (2020)
- [43] O. Boukari, H. Pais, S. Antić *et al.*, *Phys. Rev. C* **103**, 055804 (2021)
- [44] K. A. Brueckner and J. L. Gammel, *Phys. Rev.* **109**, 1023 (1958)
- [45] J. Jeukenne, A. Lejeune, and C. Mahaux, *Phys. Rep.* **25**, 83 (1976)
- [46] B. Day, *Nucl. Phys. A* **328**, 1 (1979)
- [47] C. Bloch and C. De Dominicis, *Nucl. Phys.* **10**, 509 (1959)
- [48] A. Lejeune, P. Grange, M. Martzolff *et al.*, *Nucl. Phys. A* **453**, 189 (1986)
- [49] M. Lacombe, B. Loiseau, J. M. Richard *et al.*, *Phys. Rev. C* **21**, 861 (1980)
- [50] R. B. Wiringa, R. A. Smith, and T. L. Ainsworth, *Phys. Rev. C* **29**, 1207 (1984)
- [51] S. C. Pieper, V. R. Pandharipande, R. B. Wiringa *et al.*, *Phys. Rev. C* **64**, 014001 (2001)
- [52] R. Machleidt, K. Holinde, and C. Elster, *Phys. Rep.* **149**, 1 (1987)
- [53] X. L. Shang, A. Li, Z. Q. Miao *et al.*, *Phys. Rev. C* **101**, 065801 (2020)
- [54] A. Rios, A. Polls, A. Ramos *et al.*, *Phys. Rev. C* **78**, 044314 (2008)
- [55] S. Fiorilla, N. Kaiser, and W. Weise, *Nucl. Phys. A* **880**, 65 (2012)
- [56] R. B. Wiringa, V. G. J. Stoks, and R. Schiavilla, *Phys. Rev. C* **51**, 38 (1995)
- [57] M. M. Nagels, T. A. Rijken, and J. J. de Swart, *Phys. Rev. D* **17**, 768 (1978)
- [58] P. Grangé, A. Lejeune, M. Martzolff *et al.*, *Phys. Rev. C* **40**, 1040 (1989)
- [59] W. Zuo, A. Lejeune, U. Lombardo *et al.*, *Nucl. Phys. A* **706**, 418 (2002)
- [60] Z. H. Li, U. Lombardo, H.-J. Schulze *et al.*, *Phys. Rev. C* **77**, 034316 (2008)
- [61] Z. H. Li and H.-J. Schulze, *Phys. Rev. C* **78**, 028801 (2008)
- [62] B. S. Pudliner, V. R. Pandharipande, J. Carlson *et al.*, *Phys. Rev. C* **56**, 1720 (1997)
- [63] Z.-H. Li, D.-P. Zhang, H.-J. Schulze *et al.*, *Chin. Phys. Lett.* **29**, 012101 (2012)
- [64] G. Taranto, M. Baldo, and G. F. Burgio, *Phys. Rev. C* **87**, 045803 (2013)
- [65] Q.-Y. Bu, Z.-H. Li, and H.-J. Schulze, *Chin. Phys. Lett.* **33**, 032101 (2016)
- [66] G. F. Burgio, A. Drago, G. Pagliara *et al.*, *Astrophys. J.* **860**, 139 (2018)
- [67] J.-B. Wei, A. Figura, G. F. Burgio *et al.*, *J. Phys. G* **46**, 034001 (2019)
- [68] J.-B. Wei, J.-J. Lu, G. Burgio, *et al.*, *EPJA* **56**, 1 (2020)
- [69] J. Goldstone, *Proceedings of the Royal Society of London. Series A. Mathematical and Physical Sciences* **239**, 267 (1957)
- [70] I. Bombaci and U. Lombardo, *Phys. Rev. C* **44**, 1892 (1991)
- [71] W. Zuo, I. Bombaci, and U. Lombardo, *Phys. Rev. C* **60**, 024605 (1999)
- [72] I. Bombaci, T. T. Kuo, and U. Lombardo, *Phys. Rep.* **242**, 165 (1994)
- [73] D. Logoteta, A. Perego, and I. Bombaci, *Astron. Astrophys.* **646**, A55 (2021)
- [74] T. Cheon and E. F. Redish, *Phys. Rev. C* **39**, 331 (1989)
- [75] R. Sartor, *Phys. Rev. C* **54**, 809 (1996)
- [76] X. L. Shang, J. M. Dong, W. Zuo *et al.*, *Phys. Rev. C* **103**, 034316 (2021)
- [77] D. W. E. Blatt and B. H. J. McKellar, *Phys. Rev. C* **11**, 614 (1975)
- [78] S. A. Coon, M. D. Scadron, P. C. McNamee *et al.*, *Nucl. Phys. A* **317**, 242 (1979)
- [79] X. R. Zhou, G. F. Burgio, U. Lombardo, *et al.*, *Phys. Rev. C* **69**, 018801 (2004)
- [80] Z.-H. Li and H.-J. Schulze, *Phys. Rev. C* **94**, 024322 (2016)
- [81] J.-J. Lu, Z.-H. Li, C.-Y. Chen *et al.*, *Phys. Rev. C* **98**, 064322 (2018)
- [82] A. Li, X. R. Zhou, G. F. Burgio *et al.*, *Phys. Rev. C* **81**, 025806 (2010)
- [83] G. F. Burgio, H.-J. Schulze, and A. Li, *Phys. Rev. C* **83**, 025804 (2011)
- [84] J.-J. Lu, Z.-H. Li, G. F. Burgio *et al.*, *Phys. Rev. C* **100**, 054335 (2019)